Weierstraß-Institut
für Angewandte Analysis und Stochastik

Leibniz-Institut im Forschungsverbund Berlin e. V.

Preprint ISSN 2198-5855

Divergence-preserving reconstructions on polygons and a really pressure-robust virtual element method for the Stokes problem

Derk Frerichs, Christian Merdon

submitted: February 4, 2020

Weierstrass Institute
Mohrenstr. 39
10117 Berlin
E-Mail: derk.frerichs@wias-berlin.de
christian.merdon@wias-berlin.de

No. 2683
Berlin 2020

2010 *Mathematics Subject Classification.* 65N12, 65N30, 76D07, 76D05, 76M10.

2008 *Physics and Astronomy Classification Scheme.* 47.10.ad, 47.11.Fg.

Key words and phrases. Incompressible Navier–Stokes equations, mixed virtual element method, pressure-robustness, divergence-free velocity reconstruction, polygonal meshes.

Edited by
Weierstraß-Institut für Angewandte Analysis und Stochastik (WIAS)
Leibniz-Institut im Forschungsverbund Berlin e. V.
Mohrenstraße 39
10117 Berlin
Germany

Fax: +49 30 20372-303
E-Mail: preprint@wias-berlin.de
World Wide Web: http://www.wias-berlin.de/

Divergence-preserving reconstructions on polygons and a really pressure-robust virtual element method for the Stokes problem

Derk Frerichs, Christian Merdon

ABSTRACT. Non divergence-free discretisations for the incompressible Stokes problem may suffer from a lack of pressure-robustness characterised by large discretisations errors due to irrotational forces in the momentum balance. This paper argues that also divergence-free virtual element methods (VEM) on polygonal meshes are not really pressure-robust as long as the right-hand side is not discretised in a careful manner. To be able to evaluate the right-hand side for the testfunctions, some explicit interpolation of the virtual testfunctions is needed that can be evaluated pointwise everywhere. The standard discretisation via an L^2-bestapproximation does not preserve the divergence and so destroys the orthogonality between divergence-free testfunctions and possibly eminent gradient forces in the right-hand side. To repair this orthogonality and restore pressure-robustness another divergence-preserving reconstruction is suggested based on Raviart–Thomas approximations on local subtriangulations of the polygons. All findings are proven theoretically and are demonstrated numerically in two dimensions. The construction is also interesting for hybrid high-order methods on polygonal or polyhedral meshes.

1. INTRODUCTION

Recently, the mathematical community became interested in flexible approximation methods on polygonal or polyhedral meshes. For the Stokes problem, several approaches are available, see e.g. [14, 28, 15, 13, 10, 12] and the references therein. One very popular and elegant approach is the virtual element method [6, 7] that preserve the H^1-conformity and the divergence constraint of the velocity field on the discrete level on polygonal meshes. Usually, conforming divergence-free methods are also pressure-robust as any divergence-free function is orthogonal against (pressure) gradients that appear in the momentum balance [19], in particular in the right-hand side.

However, the fact that the virtual test functions are only known at the degrees of freedom complicates the discretisation of the right-hand side. Consequently, in the context of virtual element methods the right-hand side functional

$$F(\boldsymbol{v}_h) := \int_\Omega \boldsymbol{f} \cdot \boldsymbol{v}_h \,\mathrm{d}x$$

in general cannot be evaluated exactly and has to be approximated. To do so, the information on the ansatz functions allows to compute an $\boldsymbol{L}^2$ bestapproximation $\boldsymbol{\pi}_k$ of a certain degree k. This leads to the approximative right-hand side

$$F_h(\boldsymbol{v}_h) := \int_\Omega \boldsymbol{f} \cdot \boldsymbol{\pi}_k \boldsymbol{v}_h \,\mathrm{d}x.$$

In the a priori error estimate for the velocity error $\|\nabla(\boldsymbol{u} - \boldsymbol{u}_h)\|_{L^2}$ an additional discretisation error pops up that can be quantified by the dual norm of $\boldsymbol{F} - \boldsymbol{F}_h$ with respect to the divergence-free VEM subspace $\boldsymbol{V}_{0,h}$, i.e.

$$\|\boldsymbol{F} - \boldsymbol{F}_h\|_{\boldsymbol{V}_{0,h}^\star} := \sup_{\boldsymbol{v}_h \in \boldsymbol{V}_{0,h}\setminus\{0\}} \frac{F(\boldsymbol{v}_h) - F_h(\boldsymbol{v}_h)}{\|\nabla \boldsymbol{v}_h\|_{L^2}} \lesssim \mathcal{O}(h^{k+2})|\boldsymbol{f}|_{H^{k+1}}$$

Since this consistency error enters the a priori velocity estimate with the inverse of the viscosity $1/\nu$, the velocity error might be large in case of large complicated pressures p/ν, e.g. $\boldsymbol{f} = \nabla p$ in the worst case. A pressure-robust discretisation would be pressure-independent and locking-free for $\nu \to 0$ in the sense of [3, 2], see [19, 25, 24, 17] for more details on pressure-robustness and why it is important. Although an enhanced version of the VEM achieves a discretisation error in the right-hand side of higher order, the

DOI 10.20347/WIAS.PREPRINT.2683 Berlin 2020

method is only asymptotically pressure-robust for $h \to 0$, but still can show large errors on coarser meshes which is demonstrated in the numerical examples below.

This contribution argues that uniform pressure-robustness, meaning on any mesh, can only be attained by an $\boldsymbol{H}(\mathrm{div}, \Omega)$-conforming interpolation Π that preserves the divergence of the virtual test functions. On triangles, such an interpolation is given by a standard Raviart-Thomas interpolation in the spirit of [22, 20, 23], that also can be evaluated for the virtual ansatz functions of [6] as studied in the master's thesis [16] for order $k = 2$ and proven here for arbitrary order k. On polygons, the same idea can be exploited on a subtriangulation of the polygon and requires to solve small local Dirichlet boundary value problems for each virtual test function on each polygon. This leads to the alternative right-hand side discretisation

$$\begin{aligned}\boldsymbol{F}_{\mathrm{RT}_{k-1}}(\boldsymbol{v}_h) &:= \int_\Omega \boldsymbol{f} \cdot I_{\mathrm{RT}_{k-1}} \boldsymbol{v}_h \,\mathrm{d}x \\ &= \int_\Omega \mathbb{P}\boldsymbol{f} \cdot I_{\mathrm{RT}_{k-1}} \boldsymbol{v}_h \,\mathrm{d}x \quad \text{for } \boldsymbol{v}_h \in \boldsymbol{V}_{0,h}\end{aligned}$$

and the corresponding discretisation error can be estimated by

$$\|\boldsymbol{F} - \boldsymbol{F}_{\mathrm{RT}_{k-1}}\|_{\boldsymbol{V}_{0,h}^\star} \lesssim \|h_{\mathcal{T}}(\mathbb{P}\boldsymbol{f} - \boldsymbol{\pi}_{k-2}(\mathbb{P}\boldsymbol{f}))\|_{L^2} \lesssim \nu \|h_{\mathcal{T}}^k D^{k-1} \Delta \boldsymbol{u}\|_{L^2}.$$

Here, $\mathbb{P}\boldsymbol{f} \in \boldsymbol{L}^2(\Omega)$ is the (divergence-free) Helmholtz projector of $\boldsymbol{f}$, that can be identified as $\mathbb{P}\boldsymbol{f} = -\nu\Delta\boldsymbol{u}$ when testing with divergence-free test functions, see [26] for details. Surprisingly, for the virtual element method of order $k = 2$, also a lowest order Raviart–Thomas interpolation I_{RT_0} seems enough to preserve the optimal velocity convergence order, i.e. it holds the estimate

$$\|\boldsymbol{F} - \boldsymbol{F}_{\mathrm{RT}_0}\|_{\boldsymbol{V}_{0,h}^\star} \lesssim \|h_{\mathcal{T}}^2 \mathrm{curl}(\boldsymbol{f})\|_{L^2}$$

but at the price that the pressure error converges only suboptimally with order 1. The proof employs techniques from [21].

Finally, we want to stress that the design of the reconstruction operator can be transferred also in the setting of hybrid high order methods on general meshes [28] which can be seen as a generalisation of the design in [12] on simplicial meshes. This observation together with other conclusions are reported at the end of the paper. Also, although all results are stated in two dimensions, everything can be extended to three dimensions in a straightforward way.

The rest of the paper is organised as follows. Section 2 introduces the Stokes model problem and some preliminaries. Section 3 discusses the classical virtual element discretisation and some improvements invented by the VEM community that already help to repair the lack of pressure-robustness to a certain extent. Section 4 observes and proves that a pressure-robust discretisation on shape-regular polygons is possible with the help of Raviart–Thomas interpolations which can be computed despite the virtuality of the VEM testfunctions. The resulting pressure-robust a priori estimates are shown in Section 5 as well as the surprising fact that also a standard Raviart–Thomas interpolation of lower order is enough to keep the optimal order of convergence for the velocity error. Section 6 shows some numerical examples that confirm the theoretical results. Finally, Section 7 discusses some generalisations and the relevance of the reconstruction operator for the full Navier-Stokes problem.

2. Preliminaries

This section recalls the Stokes model problem and the Helmholtz–Hodge projector which is an important tool to explain pressure-robustness and to derive pressure-robust error estimates.

2.1. **Stokes model problem.** Consider some two dimensional Liptschitz domain Ω with boundary $\partial\Omega$. The Stokes equations seek some velocity field $\boldsymbol{u} \in \boldsymbol{H}^1_0(\Omega)$ and some pressure field $p \in L^2_0(\Omega) := \{q \in L^2(\Omega) : \int_\Omega q \,\mathrm{d}x = 0\}$ such that

$$-\nu\Delta\boldsymbol{u} + \nabla p = \boldsymbol{f}, \quad \text{and} \quad \operatorname{div}\boldsymbol{u} = 0 \qquad \text{in } \Omega$$

for some given right-hand side $\boldsymbol{f} \in \boldsymbol{L}^2(\Omega)$ and positive viscosity $\nu > 0$.

The weak solution is characterised by

$$\begin{aligned} a(\boldsymbol{u},\boldsymbol{v}) + b(p,\boldsymbol{v}) &= F(v) && \text{for all } \boldsymbol{v} \in \boldsymbol{H}^1_0(\Omega),\\ b(q,\boldsymbol{u}) &= 0 && \text{for all } q \in L^2_0(\Omega) \end{aligned}$$

where

$$\begin{aligned} a(\boldsymbol{u},\boldsymbol{v}) &:= \nu \int_\Omega \nabla\boldsymbol{v} : \nabla\boldsymbol{u} \,\mathrm{d}x,\\ b(q,\boldsymbol{v}) &:= -\int_\Omega q\operatorname{div}\boldsymbol{v} \,\mathrm{d}x,\\ F(\boldsymbol{v}) &:= \int_\Omega \boldsymbol{f}\cdot\boldsymbol{v} \,\mathrm{d}x. \end{aligned}$$

From standard saddle point theroy (see e.g. [9]) it is well known that it exists a unique solution $(\boldsymbol{u}, p) \in \boldsymbol{H}^1_0(\Omega) \times L^2_0(\Omega)$ to the Stokes equations.

2.2. **Helmholtz–Hodge projector and pressure-robustness.** Recall the $\boldsymbol{L}^2$-orthogonal Helmholtz–Hodge decomposition (see e.g. [18]) that decomposes any vector field $\boldsymbol{f} \in \boldsymbol{L}^2(\Omega)$ uniquely into

$$\boldsymbol{f} = \nabla\alpha + \mathbb{P}(\boldsymbol{f}), \tag{2.1}$$

where $\alpha \in H^1(\Omega)/\mathbb{R}$, and

$$\mathbb{P}(\boldsymbol{f}) \in \boldsymbol{L}^2_\sigma(\Omega) := \{\boldsymbol{w} \in \boldsymbol{L}^2(\Omega) : (\nabla q, \boldsymbol{w}) = 0 \text{ for all } q \in H^1(\Omega)\}.$$

The latter one is called the Helmholtz–Hodge projector $\mathbb{P}(\boldsymbol{f})$ of $\boldsymbol{f}$ and is divergence-free. Also note that $\mathbb{P}(\nabla q) = 0$ for any $q \in H^1(\Omega)$.

On the continuous level the $\nabla\alpha$ part of the right-hand side in the momentum balance of the Stokes equations goes into the pressure p, whereas the Helmholtz-projector determines the velocity. Pressure-robust discretisations respect this balance and avoid an influence of α on the velocity [19, 25, 26].

Therefore, a pressure-robust discretisation is characterised by a velocity error that is independent of the exact pressure.

3. Virtual element methods for the Stokes problem

This section introduces some notation and the setup of the virtual element method for the Stokes problem as given in [5]. The last two subsections comment on known a priori estimates and an enhanced version of [6] that improves the disretisation error of the right-hand side without healing the lack of pressure-robustness completely.

3.1. **Mesh notation and assumptions.** Throughout the paper, $\mathcal{T}$ denotes a decomposition of the domain $\Omega \subset \mathbb{R}^2$ into non-overlapping simple polygons K with

$$h_K := \operatorname{diam}(K) \quad \text{and} \quad h := \sup_{K \in \mathcal{T}_h} h_K.$$

Moreover, $\mathcal{E}$ denotes the set of faces of the decomposition $\mathcal{T}$ and $\mathcal{E}(K)$ denotes the set of faces of a polygon $K \in \mathcal{T}$.

For simplicity, $\mathcal{T}$ is supposed to fulfill the following standard shape regularity properties, see e.g. [4, 5]: There exist two positive constants $\gamma_1, \gamma_2 \in \mathbb{R}$, such that each $K \in \mathcal{T}$ satisfies the assumptions

(A1) K is star-shaped with respect to a ball of radius larger or equal to $\gamma_1 h_K$,
(A2) the distance between any two vertices of K is larger or equal to $\gamma_2 h_K$.

As usual this shape regularity properties can be weakend a little, see [4, 5].

References to convergence rates in this paper always are meant with respect to a series of decompositions with uniformly bounded γ_1, γ_2. Constants hidden in $\lesssim$ may depend on these bounds but not on h.

3.2. **Virtual element method.** The virtual element method (VEM) for solving the Stokes problem given in [5] shall serve as a starting point for the new pressure-robust version.

For a fixed integer $k \in \mathbb{N}$, on each element $K \in \mathcal{T}$ the local virtual element spaces are defined by

$$\begin{aligned} \boldsymbol{V}_h^K := \Big\{ \boldsymbol{v}_h \in \boldsymbol{H}^1(K) \,:\, \boldsymbol{v}_h|_{\partial K} \in \boldsymbol{C}^0(\partial K),\, \boldsymbol{v}_h|_E \in \boldsymbol{P}_k(K) \text{ for all } E \in \mathcal{E}(K), \\ -\nu\Delta \boldsymbol{v}_h + \nabla s \in \mathcal{G}_{k-2}(T)^\perp \text{ for some } s \in L^2(K),\, \operatorname{div} \boldsymbol{v}_h \in P_{k-1}(K) \Big\}, \\ Q_h^K := P_{k-1}, \end{aligned}$$

where $P_k(K)$ and $\boldsymbol{P}_k(K)$ denote the scalar-valued and vector-valued polynomials of degree at most k on K, respectively, and $\mathcal{G}_{k-2}(K)^\perp \subset \boldsymbol{P}_{k-2}(K)$ is the $\boldsymbol{L}^2$-orthogonal complement to $\nabla P_{k-1}(K)$. This means that every vector valued polyonomial $\boldsymbol{q}_{k-2}$ of degree at most $k-2$ can be decomposed into a gradient and an orthogonal part, i.e.

$$\boldsymbol{q}_{k-2} = \nabla r_{k-1} + \boldsymbol{s}_{k-2}^\perp, \tag{3.1}$$

where $r_{k-1} \in P_{k-1}$ and $\boldsymbol{s}_{k-2}^\perp \in \mathcal{G}_{k-2}^\perp$.

For a given function $\boldsymbol{v}_h \in \boldsymbol{V}_h^K$ the following degrees of freedom are chosen:

- **D$_V$1**: the values of $\boldsymbol{v}_h$ at the vertices of the polygon K,
- **D$_V$2**: the values of $\boldsymbol{v}_h$ at $k-1$ disctinct internal points of every edge $E \in \mathcal{E}(K)$,
- **D$_V$3**: the moments

$$\int_K \boldsymbol{v}_h \cdot \boldsymbol{g}_{k-2}^\perp \,\mathrm{d}x \qquad \text{for all } \boldsymbol{g}_{k-2}^\perp \in \mathcal{G}_{k-2}^\perp,$$

- **D$_V$4**: the moments

$$\int_K \operatorname{div} \boldsymbol{v}_h \, q_{k-1} \,\mathrm{d}x \qquad \text{for all } q_{k-1} \in P_{k-1}/\mathbb{R}.$$

In addition to that, the local pressure $q_h \in Q_h^K$ is defined by the degrees of freedom

- **D$_Q$**: the moments

$$\int_K q_h \, r_{k-1} \,\mathrm{d}x \qquad \text{for all } r_{k-1} \in P_{k-1}(K).$$

Lemma 3.1. The degrees of freedom $\mathbf{D_V}$ and $\mathbf{D_Q}$ are unisolvent for the virtual space $\boldsymbol{V}_h^K$ and Q_h^K, respectively.

Proof. See Proposition 3.1 in [5]. □

The global virtual element spaces are defined as

$$\boldsymbol{V}_h := \left\{ \boldsymbol{v}_h \in \boldsymbol{H}_0^1(\Omega) \,:\, \boldsymbol{v}_h|_K \in \boldsymbol{V}_h^K \quad \text{for all } K \in \mathcal{T} \right\}$$
$$Q_h := \left\{ q_h \in L^2(\Omega) \,:\, q_h|_K \in Q_h^K \quad \text{for all } K \in \mathcal{T} \right\},$$

with global degrees of freedom as the collection of the local ones, with appropriate continuity of facial degrees of freedom $\mathbf{D_V1}$ and $\mathbf{D_V2}$ across polygonal boundaries.

Next, discrete bilinearforms are chosen. For this purpose, on each $K \in \mathcal{T}$ the energy projection $\Pi_k^{\nabla,K} : \boldsymbol{V}_h^K \to \boldsymbol{P}_k(K)$ is needed, defined as solution of

$$a^K(\boldsymbol{q}_h, \boldsymbol{v}_h - \Pi_h^{\nabla,K}\boldsymbol{v}_h) = 0 \qquad \text{for all } \boldsymbol{q}_h \in \boldsymbol{P}_k(K)$$
$$\boldsymbol{\pi}_0(\boldsymbol{v}_h - \Pi_h^{\nabla,K}\boldsymbol{v}_h) = 0,$$

where $\boldsymbol{\pi}_k$ denotes the piecewise bestapproximation into the polyonomials $\boldsymbol{P}_k$, and $a^K(\boldsymbol{u}_h, \boldsymbol{v}_h) := \nu \int_K \nabla \boldsymbol{u}_h : \nabla \boldsymbol{v}_h \,\mathrm{d}x$ for all $\boldsymbol{u}_h, \boldsymbol{v}_h \in \boldsymbol{V}_h^K$.

As shown in [5] the projection $\Pi_k^{\nabla,K}\boldsymbol{v}_h$ of any virtual function $\boldsymbol{v}_h \in \boldsymbol{V}_h^K$ can be computed using only the degrees of freedom and it holds the Poincaré inequality

$$\|\boldsymbol{v}_h - \Pi_h^{\nabla,K}\boldsymbol{v}_h\|_{L^2(K)} \lesssim h_K \|\nabla \boldsymbol{v}_h\|_{L^2(K)}. \tag{3.2}$$

The discrete bilinear forms $a_h^P : \boldsymbol{V}_h^K \times \boldsymbol{V}_h^K \to \mathbb{R}$ and $b_h^P : Q_h^K \times \boldsymbol{V}_h^K \to \mathbb{R}$ are defined by

$$a_h^K(\boldsymbol{u}_h, \boldsymbol{v}_h) := a^K\left(\Pi_k^{\nabla,K}\boldsymbol{u}_h, \Pi_k^{\nabla,K}\boldsymbol{v}_h\right) + \nu \mathcal{S}^K\left((I - \Pi_k^{\nabla,K})\boldsymbol{u}_h, (I - \Pi_k^{\nabla,K})\boldsymbol{v}_h\right),$$
$$b_h^K(q_h, \boldsymbol{v}_h) := b^K(q_h, \boldsymbol{v}_h) := \int_K q_h \mathrm{div} \boldsymbol{v}_h \,\mathrm{d}x$$

for all $\boldsymbol{u}_h, \boldsymbol{v}_h \in \boldsymbol{V}_h^K, q_h \in Q_h^K$, where $S^K : \boldsymbol{V}_h^K \times \boldsymbol{V}_h^K \to \mathbb{R}$ is some stability bilinear form. Possible choices for the stability bilinear form are given for instance in [8]. Since the choice of the stability bilinear form does not matter for our purpose, we simply use the vector product of the evaluations of the degrees of freedoms

$$\mathcal{S}^K(\boldsymbol{u}_h, \boldsymbol{v}_h) = \mathbf{D_V}(\boldsymbol{u}_h) \cdot \mathbf{D_V}(\boldsymbol{v}_h).$$

The global bilinearforms $a_h(\cdot,\cdot)$ and $b_h(\cdot,\cdot)$ are the sums over the local contributions. The 'classical' discretisation of the VEM (see e.g. [5]) right-hand side reads

$$\boldsymbol{F}_h(\boldsymbol{v}_h) := \int_\Omega \boldsymbol{\pi}_{k-2}\boldsymbol{f} \cdot \boldsymbol{v}_h = \int_\Omega \boldsymbol{f} \cdot \boldsymbol{\pi}_{k-2}\boldsymbol{v}_h$$

where $\boldsymbol{\pi}_{k-2}$ is the piecewise $\boldsymbol{L}^2$-bestapproximtion onto the vector-valued polynomials of degree $k-2$. Later, alternative (pressure-robust) discretisations are introduced. However, we first turn our focus on the possible a priori error estimates one obtains with this classical choice.

It can be easily checked that all the bilinear forms and the projections can be evaluated only with the degrees of freedom, see e.g. [11] for details. Therefore, the discrete problem reads as follows: Find $(\boldsymbol{u}_h, p_h) \in$

$\boldsymbol{V}_h \times Q_h$ such that

$$\begin{aligned} a_h(\boldsymbol{u}_h, \boldsymbol{v}_h) + b_h(p_h, \boldsymbol{v}_h) &= F(\boldsymbol{v}_h) && \text{for all } \boldsymbol{v}_h \in \boldsymbol{V}_h \\ b_h(q_h, \boldsymbol{u}_h) &= 0 && \text{for all } q_h \in Q_h. \end{aligned}$$

The discrete problem has a unique (but virtual) solution which is pointwise divergence free [5].

3.3. **A priori error estimates.** This section recalls a priori error estimates for the velocity and pressure of the VEM. To focus on the discretisation error of the right-hand side consider the following dual norms

$$\begin{aligned} \|\boldsymbol{F} - \boldsymbol{F}_h\|_{\boldsymbol{V}_{0,h}^\star} &:= \sup_{\boldsymbol{v}_h \in \boldsymbol{V}_{0,h}\setminus\{0\}} \frac{F(\boldsymbol{v}_h) - F_h(\boldsymbol{v}_h)}{\|\nabla \boldsymbol{v}_h\|_{L^2}}, \\ \|\boldsymbol{F} - \boldsymbol{F}_h\|_{\boldsymbol{V}_h^\star} &:= \sup_{\boldsymbol{v}_h \in \boldsymbol{V}_h\setminus\{0\}} \frac{F(\boldsymbol{v}_h) - F_h(\boldsymbol{v}_h)}{\|\nabla \boldsymbol{v}_h\|_{L^2}}. \end{aligned}$$

Here $\boldsymbol{V}_{0,h} := \{\boldsymbol{v}_h \in \boldsymbol{V}_h : \operatorname{div}(\boldsymbol{v}_h) = 0\}$ denotes the subspace of divergence-free virtual functions. The first dual norm refers to testing only with divergence-free velocity test functions and the second dual norm to testing with arbitrary ones that appear in a priori pressure estimates.

Theorem 3.2 (A priori estimates)**.** Under sufficient regularity assumptions on $\boldsymbol{u}$ and p, there holds

$$\begin{aligned} \|\nabla(\boldsymbol{u} - \boldsymbol{u}_h)\|_{L^2} &\lesssim \inf_{\boldsymbol{v}_h \in \boldsymbol{V}_h} \|\nabla(\boldsymbol{u} - \boldsymbol{v}_h)\|_{L^2} + \inf_{\boldsymbol{v}_h \in \boldsymbol{P}_k(\mathcal{T})} \|\nabla_h(\boldsymbol{u} - \boldsymbol{v}_h)\|_{L^2} + \frac{1}{\nu}\|\boldsymbol{F} - \boldsymbol{F}_h\|_{\boldsymbol{V}_{0,h}^\star} \\ \|p - p_h\|_{L^2} &\lesssim \inf_{q_h \in Q_h} \|p - q_h\|_{L^2} + \nu \inf_{\boldsymbol{v}_h \in \boldsymbol{V}_h} \|\nabla(\boldsymbol{u} - \boldsymbol{v}_h)\|_{L^2} + \nu \inf_{\boldsymbol{v}_h \in \boldsymbol{P}_k(\mathcal{T})} \|\nabla_h(\boldsymbol{u} - \boldsymbol{v}_h)\|_{L^2} \\ &\quad + \|\boldsymbol{F} - \boldsymbol{F}_h\|_{\boldsymbol{V}_h^\star} \end{aligned}$$

where ∇_h is the piecewise gradient with respect to $\mathcal{T}$. Since the bestapproximations converge optimally ([5, 4]), the VEM has the optimal velocity and pressure convergence order k whenever the consistency errors of the right-hand side discretisation is of the right order.

Proof. See [5, 4] and adapt to dual norms. □

Lemma 3.3 (Right-hand side discretisation consistency error)**.** The consistency errors of the classical right-hand side discretisation are bounded by

$$\|\boldsymbol{F} - \boldsymbol{F}_h\|_{\boldsymbol{V}_{0,h}^\star} \leqslant \|\boldsymbol{F} - \boldsymbol{F}_h\|_{\boldsymbol{V}_h^\star} \lesssim \|h_{\mathcal{T}}(\boldsymbol{f} - \boldsymbol{\pi}_{k-2}\boldsymbol{f})\|_{L^2} \lesssim \|h_{\mathcal{T}}^k \mathrm{D}^{k-1}\boldsymbol{f}\|_{L^2}$$

where the last estimate requires $\boldsymbol{f} \in \boldsymbol{H}^{k-1}(\Omega)$ and D^{k-1} collects all derivatives of order $k-1$.

Proof. This follows directly from the approximation properties of the $\boldsymbol{L}^2$ bestapproximation $\boldsymbol{\pi}_{k-2}$, see e.g. [4] for details. □

Remark 3.4 (Classical VEM is not pressure-robust)**.** Although the virtual element method is divergence-free, it is in general not pressure-robust with the classical right-hand side discretisation. This drawback can be seen e.g. when $\boldsymbol{f} = \nabla q$ for some $q \notin P_{k-1}$ and small viscosity parameters ν. Then, the method shows a locking-phenomenon for $\nu \to 0$ as it is also observed for classical finite element methods that are not divergence-free, see e.g. [2, 19] for a comprehensive introduction. The reason for that is that the operator $\boldsymbol{\pi}_{k-2}$ alters the divergence and therefore destroys the orthogonality between divergence-free functions and gradient forces. The numerical examples below demonstrate this lack of pressure-robustness.

3.4. **Extended virtual ansatz spaces.** One way of rendering the method more robust against gradient forces is to enlarge the order of the projection $\boldsymbol{\pi}_s$ used in the right-hand side discretisation. With the so called enhanced spaces introduced in [6] it is possible to employ $\boldsymbol{\pi}_k \boldsymbol{v}_h$ instead of $\boldsymbol{\pi}_{k-2}\boldsymbol{v}_h$.

For each $K \in \mathcal{T}$ the local enlarged virtual element space is given by

$$\boldsymbol{U}_h^K := \Big\{ \boldsymbol{v}_h \in \boldsymbol{H}^1(K) \,:\, \boldsymbol{v}_h|_{\partial K} \in \boldsymbol{C}^0(\partial K),\, \boldsymbol{v}_h|_E \in \boldsymbol{P}_k(K) \text{ for all } E \in \mathcal{E}(K), \\ -\nu\Delta \boldsymbol{v}_h + \nabla s \in \mathcal{G}_k(K)^\perp \text{ for some } s \in L^2(K),\, \operatorname{div} \boldsymbol{v}_h \in P_{k-1}(K) \Big\},$$

where the order of the space $\mathcal{G}_s^\perp$ was increased from $k-2$ to k.

This enlarged space can now be restricted to the enhanced space

$$W_h^K := \Big\{ \boldsymbol{v}_h \in \boldsymbol{U}_h^K \,:\, \Big(\boldsymbol{v}_h - \Pi_k^{\nabla,K}\boldsymbol{v}_h, \boldsymbol{g}_k^\perp\Big)_{L^2(K)} = 0 \text{ for all } \boldsymbol{g}_k^\perp \in \mathcal{G}_k^\perp/\mathcal{G}_{k-2}^\perp \Big\}.$$

This space has the interesting properties that it has the same dimension as the classical virtual element space, but additionally allows to compute the L^2-projection onto polynomials of degree k, see e.g. [6, 1] for more details.

The discretisation of the right-hand side for the enhanced space then reads

$$\boldsymbol{F}_h^e(\boldsymbol{v}_h) := \int_\Omega \boldsymbol{\pi}_k \boldsymbol{f} \cdot \boldsymbol{v}_h = \int_\Omega \boldsymbol{f} \cdot \boldsymbol{\pi}_k \boldsymbol{v}_h.$$

This discretisation leads to a $(k+2)$-order consistency error, i.e.

$$\|\boldsymbol{F} - \boldsymbol{F}_h^e\|_{\boldsymbol{V}_{0,h}^\star} \leqslant \|\boldsymbol{F} - \boldsymbol{F}_h^e\|_{\boldsymbol{V}_h^\star} \lesssim \|h_{\mathcal{T}}(\boldsymbol{f} - \boldsymbol{\pi}_k \boldsymbol{f})\|_{L^2} \lesssim \|h_{\mathcal{T}}^{k+2} \mathrm{D}^{k+1} \boldsymbol{f}\|_{L^2},$$

and hence the velocity error can be bounded by

$$\|\nabla(\boldsymbol{u} - \boldsymbol{u}_h)\|_{L^2} \lesssim \inf_{\boldsymbol{v}_h \in \boldsymbol{V}_h} \|\nabla(\boldsymbol{u} - \boldsymbol{v}_h)\|_{L^2} + \inf_{\boldsymbol{v}_h \in \boldsymbol{P}_k(\mathcal{T})} \|\nabla_h(\boldsymbol{u} - \boldsymbol{v}_h)\|_{L^2} + \frac{1}{\nu}\|h_{\mathcal{T}}^{k+2}\mathrm{D}^{k+1}\boldsymbol{f}\|_{L^2}.$$

Remark 3.5 (Only asymptotic pressure-robustness)**.** As for the classical VEM the enhanced VEM is not pressure-robust. Consider again the situation $\boldsymbol{f} = \nabla q$ for some $q \notin P_{k+1}$ and small viscosity parameters ν. Then, on a fixed mesh, the method still shows the same locking-behaviour for $\nu \to 0$. However, for $h \to 0$, the discretisation error converges with a faster rate and renders the enhanced VEM at least asymptotically pressure-robust.

Uniform pressure-robustness, in particular on coarse grids, requires the replacement of $\boldsymbol{\pi}_k$ by some operator that preserves the divergence of $\boldsymbol{v}_h$. This is the goal of the next section.

4. Divergence-preserving reconstruction operators on polygons

This section describes the design of a reconstruction operator that is $H(\operatorname{div})$-conforming and preserves the divergence of the virtual functions for all polygons $K \in \mathcal{T}$. The main idea is to employ a subtriangulation of each polygon and to compute a suitable Raviart–Thomas interpolation on that subtriangulation $\mathcal{T}(K)$.

4.1. **Raviart–Thomas finite element space and interpolation.** The Raviart–Thomas finite element space of order m on a subtriangulation $\mathcal{T}(K)$ is defined by

$$\mathrm{RT}_m(\mathcal{T}(K)) := \Big\{ \boldsymbol{w}_h \in \boldsymbol{P}_{m+1}(\mathcal{T}(K)) \cap H(\operatorname{div}, K) \,:\, \forall T \in \mathcal{T}(K)\, \exists \boldsymbol{a} \in \boldsymbol{P}_m(T),\, b \in P_m(T), \\ \boldsymbol{w}_h|_T(\boldsymbol{x}) = \boldsymbol{a}(\boldsymbol{x}) + b(\boldsymbol{x})\boldsymbol{x} \Big\}.$$

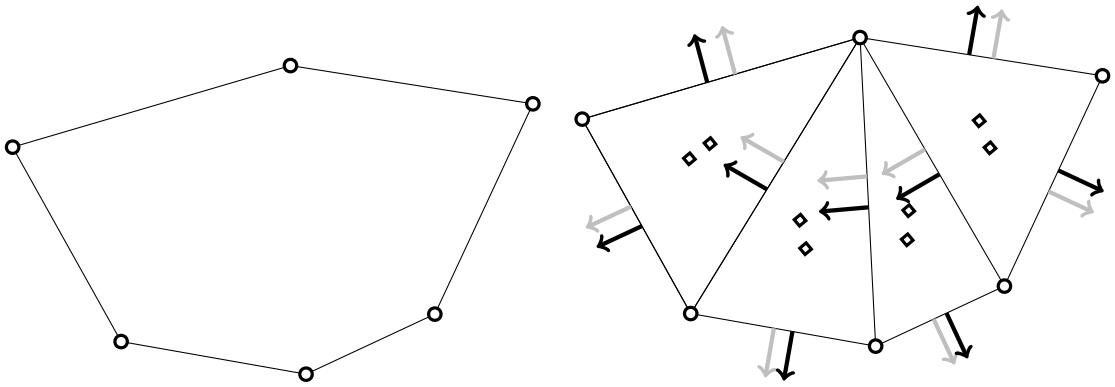

FIGURE 4.1. A polygon (left) and a possible subtriangulation (right) and its facial (arrows) and interior (squares) degrees of freedom for the Raviart–Thomas interpolation of order 1. Light-gray arrows relate to the degrees of freedom of the lowest-order Raviart–Thomas space.

The standard Raviart-Thomas interpolation $\Pi_{\mathrm{RT}_m}\boldsymbol{v}_h \in \mathrm{RT}_m(\mathcal{T}(K))$ of some (virtual) function $\boldsymbol{v}_h \in \boldsymbol{V}_h$ is defined by

$$\int_T (\Pi_{\mathrm{RT}_m}\boldsymbol{v}_h - \boldsymbol{v}_h)\cdot\boldsymbol{q}_h \,\mathrm{d}s = 0 \qquad \text{for all } \boldsymbol{q}_h \in \boldsymbol{P}_{m-1}(\mathcal{T}(P)),$$
$$\int_E (\Pi_{\mathrm{RT}_m}\boldsymbol{v}_h - \boldsymbol{v}_h)\cdot\boldsymbol{n}q_h \,\mathrm{d}s = 0 \qquad \text{for all } E \in \mathcal{E}(\mathcal{T}(P)) \text{ and } q_h \in P_m(E).$$

Here $\mathcal{E}(\mathcal{T}(P))$ denotes the set of edges in the subtriangulation $\mathcal{T}(P)$. The following lemma collects the well-known properties of the Raviart–Thomas standard interpolation.

Lemma 4.1 (Properties of the Raviart–Thomas standard interpolation)**.** For any $\boldsymbol{V}_h \in \boldsymbol{V}_h$, there holds

(i) $$\mathrm{div}(\Pi_{\mathrm{RT}_m}(\boldsymbol{v}_h)) = \pi_m(\mathrm{div}(\boldsymbol{v}_h))$$
(ii) $$\|\boldsymbol{v}_h - \Pi_{\mathrm{RT}_m}\boldsymbol{v}_h\|_{L^2(K)} \lesssim \|h_{\mathcal{T}(K)}\nabla\boldsymbol{v}_h\|_{L^2(K)} \leqslant h_K\|\nabla\boldsymbol{v}_h\|_{L^2(K)},$$
(iii) if $m>0$: $$\int_K (\boldsymbol{v}_h - \Pi_{\mathrm{RT}_m}\boldsymbol{v}_h)\cdot\boldsymbol{q}_h \,\mathrm{d}x = 0 \quad \text{for all } \boldsymbol{q}_h \in \boldsymbol{P}_{m-1}(\mathcal{T}(K)).$$

Proof. See textbooks like e.g. [9]. □

Note, that the Raviart–Thomas standard interpolation of some virtual function cannot be calculated in general (see Remark 4.3 for an exception on triangles). Hence, one has to devise a strategy based on the known degrees of freedom. The goal of the design below is to ensure crucial properties of the Raviart–Thomas standard interpolation.

4.2. **Design of reconstruction operator by local minimisation problems.** On a fixed subtriangulation $\mathcal{T}(K)$ of a polygon K (such that no additional nodes on ∂K are introduced), the local reconstruction of some local basis function $\boldsymbol{v}_h$ is defined by

$$I_{\mathrm{RT}_m}(\boldsymbol{v}_h) := \operatorname*{argmin}_{\boldsymbol{w}_h\in W_h(K,\boldsymbol{v}_h,m)} \|\Pi_k^{\nabla,K}(\boldsymbol{v}_h) - \boldsymbol{w}_h\|_{L^2(K)} \tag{4.1}$$

where

$$W_h(K, \boldsymbol{v}_h, m) := \Big\{ \boldsymbol{w}_h \in \mathrm{RT}_m(\mathcal{T}(K)) : \forall q_h \in P_m(\mathcal{T}(K)),\ \int_K \operatorname{div}(\boldsymbol{v}_h - \boldsymbol{w}_h) q_h \,\mathrm{d}x = 0$$
$$\text{and } \forall \boldsymbol{q}_h^\perp \in \mathcal{G}_{m-1}^\perp,\ \int_K (\boldsymbol{v}_h - \boldsymbol{w}_h) \cdot \boldsymbol{q}_h^\perp \,\mathrm{d}x = \boldsymbol{0}$$
$$\text{and } \forall E \in \mathcal{E}(K), q_h \in P_m(E),\ \int_E (\boldsymbol{v}_h - \boldsymbol{w}_h) \cdot \boldsymbol{n}\, q_h \,\mathrm{d}s = 0 \Big\}.$$

The following lemma states that the set $W_h(K, \boldsymbol{v}_h, m)$ is non-empty, and the minimisation problem defining $I_{\mathrm{RT}_m}(\boldsymbol{v}_h)$ therefore is well-defined. Remark 4.4 however shows that we have to choose $m \leqslant k-1$ and the a priori error estimates in Section 5 show that only $m \in \{k-2, k-1\}$ are reasonable choices.

Lemma 4.2 ($W_h(K, \boldsymbol{v}_h, m)$ is non-empty)**.** The piecewise standard Raviart-Thomas interpolation $\Pi_{\mathrm{RT}_m} \boldsymbol{v}_h$ is included in $W_h(K, \boldsymbol{v}_h, m)$. Moreover, if K is a triangle, it holds $W_h(K, \boldsymbol{v}_h, m) = \{\Pi_{\mathrm{RT}_m} \boldsymbol{v}_h\}$.

Proof. It suffices to show that the moments of the divergence are preserved by the standard interpolation. An integration by parts indeed shows, for any $q_h \in P_m(\mathcal{T}(K))$,

$$\int_K \operatorname{div}(\boldsymbol{v}_h - \Pi_{\mathrm{RT}_m} \boldsymbol{v}_h) q_h \,\mathrm{d}x = -\int_K (\boldsymbol{v}_h - \Pi_{\mathrm{RT}_m} \boldsymbol{v}_h) \cdot \nabla q_h \,\mathrm{d}x + \int_{\partial K} (\Pi_{\mathrm{RT}_m} \boldsymbol{v}_h - \boldsymbol{v}_h) \cdot \boldsymbol{n} q_h \,\mathrm{d}s$$
$$= 0$$

due to $\nabla q_h \in \boldsymbol{P}_{m-1}(\mathcal{T}(P))$ and the properties of the standard interpolation. For $m = 0$, the first property of the standard interpolation is not available, but also the integral over K on the right-hand side vanishes. This shows $\Pi_{\mathrm{RT}_m} \boldsymbol{v}_h \in W_h(K, \boldsymbol{v}_h, m)$.

On a triangle (with no interior edges), a similar backward calculation employing the splitting (3.1) shows that every $w_h \in W_h(K, \boldsymbol{v}_h, m)$ satisfies the properties of $\Pi_{\mathrm{RT}_m} \boldsymbol{v}_h$, and hence $W_h(K, \boldsymbol{v}_h, m) = \{\Pi_{\mathrm{RT}_m} \boldsymbol{v}_h\}$. □

Remark 4.3. In general the standard interpolation $\Pi_{\mathrm{RT}_m} \boldsymbol{v}_h$ of Lemma 4.2 is not computable due to the virtuality of $\boldsymbol{v}_h$. However, if K is a triangle the standard interpolation is directly computable up to degree $m \leqslant k-1$, due to the explanations in the next remark.

Remark 4.4 (Constraints are computable for $m \leqslant k-1$)**.** Observe, that the computation of $I_{\mathrm{RT}_m}(\boldsymbol{v}_h)$ up to degree $m \leqslant k-1$ for any virtual function $\boldsymbol{v}_h \in \boldsymbol{V}_h$ is possible and only involves the evaluation of the degrees of freedom of $\boldsymbol{v}_h$. Indeed, the divergence is a polynomial of degree at most $k-1$ and is explicitly available using only **D$_\mathbf{V}$1**, **D$_\mathbf{V}$2** and **D$_\mathbf{V}$4** (see [11]), and hence

$$\int_K \operatorname{div}(\boldsymbol{v}_h - \boldsymbol{w}_h) q_h \,\mathrm{d}x = 0 \text{ for all } q_h \in P_m(\mathcal{T}(K))$$

is an integral over polynomials that can be computed.

The integrals related to the space $\mathcal{G}_{m-1}^\perp$ are also directly available from **D$_\mathbf{V}$3** up to degree $m \leqslant k-1$ (this condition in fact prohibits to choose m larger than $k-1$).

Finally, since $\boldsymbol{v}_h$ along the boundary is a polynomial of degree at most k also the boundary integral

$$\int_E (\boldsymbol{w}_h \cdot \boldsymbol{n}) q_h \,\mathrm{d}s = \int_E (\boldsymbol{v}_h \cdot \boldsymbol{n}) q_h \,\mathrm{d}s \text{ for all } E \in \mathcal{E}(\partial K) \text{ and } q_h \in P_m(E)$$

is computable. Please confer to [16] for more details and instructions for the implementation in the case $k = 2$.

Remark 4.5. It is possible to fix all degrees of freedom related to the lowest order Raviart–Thomas functions (gray arrows in Figure 4.1 for $m = 1$) separately via the preservation of the integral mean of the polynomial divergence of the virtual function $\boldsymbol{V}_h$. This slightly reduces the costs of the local minimisation problems. However, please note that in any case the costs of the local minimisation problems are comparable to the costs of the computation of $\Pi_k^{\nabla,K}$ and hence do not cause severe computational overhead.

Remark 4.6. It is also possible to replace the finite element spaces RT_m by the slightly larger Brezzi–Douglas–Marini spaces BDM_{m+1}, which may offer a slightly better divergence-free postprocessing of the solution $\boldsymbol{u}_h$.

The following Lemma summarises the properties that can be expected from this strategy.

Theorem 4.7 (Properties of the reconstruction)**.** For any $\boldsymbol{v}_h \in \boldsymbol{V}_h(K)$, there holds

$$(i) \qquad \mathrm{div}(I_{\mathrm{RT}_m}(\boldsymbol{v}_h)) = \pi_m(\mathrm{div}(\boldsymbol{v}_h))$$

$$(ii) \qquad \|\boldsymbol{v}_h - I_{\mathrm{RT}_m}\boldsymbol{v}_h\|_{L^2(K)} \lesssim h_K \|\nabla \boldsymbol{v}_h\|_{L^2(K)},$$

$$(iii) \qquad \text{if } m > 0: \quad \int_K (\boldsymbol{v}_h - I_{\mathrm{RT}_m}\boldsymbol{v}_h)\cdot \boldsymbol{q}_h \,\mathrm{d}x = 0 \quad \text{for all } \boldsymbol{q}_h \in \boldsymbol{P}_{m-1}(K).$$

Proof. Property (i) directly follows from the definition of $W_h(K, \boldsymbol{v}_h, m)$.

For the proof of (ii), consider the piecewise RT_m standard interpolation $\Pi_{\mathrm{RT}_m}\boldsymbol{v}_h$ of $\boldsymbol{v}_h$ on the subtriangulation and once again note that $\Pi_{\mathrm{RT}_m}\boldsymbol{v}_h \in \boldsymbol{W}_h(K, \boldsymbol{v}_h, m)$. Since

$$(I_{\mathrm{RT}_m}\boldsymbol{v}_h - \Pi_k^{\nabla,K}(\boldsymbol{v}_h), \boldsymbol{w}_h) = 0 \quad \text{for all } w_h \in \boldsymbol{W}_h(K, \boldsymbol{v}_h, m)$$

by (4.1), we obtain for $\boldsymbol{w_h} = I_{\mathrm{RT}_m}\boldsymbol{v}_h$ and $\boldsymbol{w}_h = \Pi_{\mathrm{RT}_m}\boldsymbol{v}_h$

$$\begin{aligned}\|I_{\mathrm{RT}_m}\boldsymbol{v}_h - \Pi_{\mathrm{RT}_m}\boldsymbol{v}_h\|^2_{L^2(K)} &= (I_{\mathrm{RT}_m}\boldsymbol{v}_h - \Pi_{\mathrm{RT}_m}\boldsymbol{v}_h, I_{\mathrm{RT}_m}\boldsymbol{v}_h - \Pi_{\mathrm{RT}_m}\boldsymbol{v}_h)\\ &= (\Pi_k^{\nabla,K}(\boldsymbol{v}_h) - \Pi_{\mathrm{RT}_m}\boldsymbol{v}_h, I_{\mathrm{RT}_m}\boldsymbol{v}_h - \Pi_{\mathrm{RT}_m}\boldsymbol{v}_h)\\ &\leqslant \|\Pi_k^{\nabla,K}(\boldsymbol{v}_h) - \Pi_{\mathrm{RT}_m}\boldsymbol{v}_h\|_{L^2(K)}\|I_{\mathrm{RT}_m}\boldsymbol{v}_h - \Pi_{\mathrm{RT}_m}\boldsymbol{v}_h\|_{L^2(K)}.\end{aligned}$$

This, a triangle inequality and the first-order approximation properties of $\Pi_k^{\nabla}(\boldsymbol{v}_h)$ (see (3.2)) and $\Pi_{\mathrm{RT}_m}\boldsymbol{v}_h$ (piecewise for each subtriangle, see Lemma 4.1.(ii)) show

$$\|I_{\mathrm{RT}_m}\boldsymbol{v}_h - \Pi_{\mathrm{RT}_m}\boldsymbol{v}_h\|_{L^2(K)} \leqslant \|\Pi_k^{\nabla,K}(\boldsymbol{v}_h) - \Pi_{\mathrm{RT}_m}\boldsymbol{v}_h\|_{L^2(K)} \lesssim h_K\|\nabla \boldsymbol{v}_h\|_{L^2(K)}.$$

Another triangle inequality gives the desired result (ii).

For the proof of (iii), consider any $\boldsymbol{q}_h \in \boldsymbol{P}_{m-1}(K)$ and its decomposition (3.1) into some $r_h \in P_m(K)$ and $\boldsymbol{s}_h^\perp \in \mathcal{G}_{m-1}^\perp$ such that

$$\boldsymbol{q}_h = \nabla r_h + \boldsymbol{s}_h^\perp.$$

Then, an integration by parts shows

$$\int_K (\boldsymbol{v}_h - I_{\mathrm{RT}_m}\boldsymbol{v}_h)\boldsymbol{q}_h \,\mathrm{d}x = -\int_K \mathrm{div}(\boldsymbol{v}_h - I_{\mathrm{RT}_m}\boldsymbol{v}_h) r_h \,\mathrm{d}x + \int_K (\boldsymbol{v}_h - I_{\mathrm{RT}_m}\boldsymbol{v}_h)\boldsymbol{s}_h^\perp \,\mathrm{d}x.$$

Both integrals vanish due to $I_{\mathrm{RT}_m}\boldsymbol{v}_h \in W_h(K, \boldsymbol{v}_h, m)$. □

5. Pressure-robust a priori error estimates

This section shows pressure-robust estimates for the discretisation error of the right-hand side. Together with Theorem 3.2 convergence rates for the modified method can be derived.

5.1. **Estimates for $I_{\mathrm{RT}_{k-1}}$.** Consider the modified right-hand side discretisation

$$\boldsymbol{F}_{\mathrm{RT}_{k-1}}(\boldsymbol{v}_h) := \int_\Omega \boldsymbol{f} \cdot I_{\mathrm{RT}_{k-1}}(\boldsymbol{v}_h)\,\mathrm{d}x.$$

Lemma 5.1 (Modified right-hand side discretisation consistency error)**.** The consistency error of the modified right-hand side discretisation is bounded by

$$\|\boldsymbol{F} - \boldsymbol{F}_{\mathrm{RT}_{k-1}}\|_{\boldsymbol{V}_{0,h}^\star} := \sup_{\boldsymbol{V}_h \in \boldsymbol{V}_h\setminus\{0\}} \frac{\boldsymbol{F}(\boldsymbol{v}_h) - \boldsymbol{F}_{\mathrm{RT}_{k-1}}(\boldsymbol{v}_h)}{\|\nabla \boldsymbol{v}_h\|_{L^2}} \lesssim \|h_{\mathcal{T}}(\mathbb{P}\boldsymbol{f} - \boldsymbol{\pi}_{k-2}(\mathbb{P}\boldsymbol{f}))\|_{L^2},$$
$$\|\boldsymbol{F} - \boldsymbol{F}_{\mathrm{RT}_{k-1}}\|_{\boldsymbol{V}_h^\star} := \sup_{\boldsymbol{V}_h \in \boldsymbol{V}_h\setminus\{0\}} \frac{\boldsymbol{F}(\boldsymbol{v}_h) - \boldsymbol{F}_{\mathrm{RT}_{k-1}}(\boldsymbol{v}_h)}{\|\nabla \boldsymbol{v}_h\|_{L^2}} \lesssim \|h_{\mathcal{T}}(\boldsymbol{f} - \boldsymbol{\pi}_{k-2}\boldsymbol{f})\|_{L^2}$$

where $\boldsymbol{\pi}_{-1} \equiv 0$. If $\Delta \boldsymbol{u} \in H^{k-1}$, then it holds

$$\|\boldsymbol{F} - \boldsymbol{F}_{\mathrm{RT}_{k-1}}\|_{\boldsymbol{V}_{0,h}^\star} \lesssim \nu \|h_{\mathcal{T}}^k D^{k-1} \Delta \boldsymbol{u}\|_{L^2}.$$

Proof. Indeed, for any (divergence-free) $\boldsymbol{v}_h \in \boldsymbol{V_{0,h}}$, it holds

$$\int_\Omega (\boldsymbol{f} - \mathbb{P}\boldsymbol{f}) \cdot (\boldsymbol{v}_h - I_{\mathrm{RT}_{k-1}}\boldsymbol{v}_h)\,dx = 0.$$

This and the properties (i)-(iii) of Lemma 4.7 yield

$$\begin{aligned}
\boldsymbol{F}(\boldsymbol{v}_h) - \boldsymbol{F}_{\mathrm{RT}_{k-1}}(\boldsymbol{v}_h) &= \int_\Omega \mathbb{P}\boldsymbol{f} \cdot (\boldsymbol{v}_h - I_{\mathrm{RT}_{k-1}}\boldsymbol{v}_h)\,\mathrm{d}x \\
&= \int_\Omega (\mathbb{P}\boldsymbol{f} - \boldsymbol{\pi}_{k-2}(\mathbb{P}\boldsymbol{f})) \cdot (\boldsymbol{v}_h - I_{\mathrm{RT}_{k-1}}\boldsymbol{v}_h)\,\mathrm{d}x \\
&\lesssim \sum_{K\in\mathcal{T}} \|\mathbb{P}\boldsymbol{f} - \boldsymbol{\pi}_{k-2}(\mathbb{P}\boldsymbol{f})\|_{L^2(K)} \|\boldsymbol{v}_h - I_{\mathrm{RT}_{k-1}}\boldsymbol{v}_h\|_{L^2(K)} \\
&\lesssim \sum_{K\in\mathcal{T}} h_P \|\mathbb{P}\boldsymbol{f} - \boldsymbol{\pi}_{k-2}(\mathbb{P}\boldsymbol{f})\|_{L^2(K)} \|\nabla \boldsymbol{v}_h\|_{L^2(P)} \\
&\leqslant \|h_{\mathcal{T}}(\mathbb{P}\boldsymbol{f} - \boldsymbol{\pi}_{k-2}(\mathbb{P}\boldsymbol{f})\|_{L^2} \|\nabla \boldsymbol{v}_h\|_{L^2}.
\end{aligned}$$

Since also $(\mathbb{P}\boldsymbol{f} + \nu\Delta\boldsymbol{u}, \boldsymbol{v}_h - I_{\mathrm{RT}_{k-1}}\boldsymbol{v}_h)_{L^2} = 0$, the same calculation can be performed with $\mathbb{P}\boldsymbol{f}$ replaced by $-\nu\Delta\boldsymbol{u}$ and leads to

$$\boldsymbol{F}(\boldsymbol{v}_h) - \boldsymbol{F}_{\mathrm{RT}_{k-1}}(\boldsymbol{v}_h) \lesssim \nu \|h_{\mathcal{T}}(\Delta\boldsymbol{u} - \boldsymbol{\pi}_{k-2}(\Delta\boldsymbol{u}))\|_{L^2} \|\nabla \boldsymbol{v}_h\|_{L^2} \lesssim \nu \|h_{\mathcal{T}}^k D^{k-1}\Delta\boldsymbol{u}\|_{L^2} \|\nabla \boldsymbol{v}_h\|_{L^2}.$$

For (non divergence-free) $\boldsymbol{v}_h \in \boldsymbol{V}_h$, one has to do the same calculation with $\boldsymbol{f}$ instead of $\mathbb{P}\boldsymbol{f}$. □

Hence, the reconstruction operator with $m = k-1$ results in a discretisation error of optimal order that is pressure-robust.

5.2. **Alternative estimate for $m = 0$.** Consider the lowest-order interpolation

$$I_{\mathrm{RT}_0}(\boldsymbol{v}_h) := \operatorname*{argmin}_{\boldsymbol{w}_h \in W_h(K, \boldsymbol{v}_h, 0)} \|\Pi_k^{\nabla,K}(\boldsymbol{v}_h) - \boldsymbol{w}_h\|_{L^2(K)}.$$

Theorem 5.2. Given some right-hand side $\boldsymbol{f}$ with $\boldsymbol{f} \in H(\mathrm{curl}, \Omega)$, it holds

$$\|\boldsymbol{F} - \boldsymbol{F}_{\mathrm{RT}_0}\|_{\boldsymbol{V}_{0,h}^\star} \lesssim \|h_{\mathcal{T}}^2 \mathrm{curl}(\boldsymbol{f})\|_{L^2}.$$

Proof. The proof is based on the same idea as the proof in [21, Theorem 7 (for $I = 1$ and $\Pi = I_{\mathrm{RT}_0}$)] . Indeed, due to $\boldsymbol{v}_h \in \boldsymbol{V}_{0,h}$ and $I_{\mathrm{RT}_0}\boldsymbol{v}_h$ being divergence-free, it holds $\boldsymbol{v}_h - I_{\mathrm{RT}_0}\boldsymbol{v}_h = \mathrm{curl}\psi$ for some $\psi \in H^1_0(\Omega) \cap H^2(\Omega)$, and hence

$$\begin{aligned}\boldsymbol{F}(\boldsymbol{v}_h) - \boldsymbol{F}_{\mathrm{RT}_0}(\boldsymbol{v}_h) &= \int_\Omega \boldsymbol{f} \cdot (\boldsymbol{v}_h - I_{\mathrm{RT}_0}\boldsymbol{v}_h)\,\mathrm{d}x \\ &= \int_\Omega \boldsymbol{f} \cdot \mathrm{curl}(\psi - I_{\mathcal{L}}\psi)\,\mathrm{d}x \\ &= -\int_\Omega \mathrm{curl}(\boldsymbol{f}) \cdot (\psi - I_{\mathcal{L}}\psi)\,\mathrm{d}x\end{aligned}$$

where $I_{\mathcal{L}}\psi$ is the nodal interpolation due to the commuting properties of the de Rham complex (on sub-triangles) $\mathrm{curl}(I_{\mathcal{L}}\psi) = I_{\mathrm{RT}_0}(\mathrm{curl}\psi) = 0$. Standard elementwise interpolation estimates then result in

$$\begin{aligned}\boldsymbol{F}(\boldsymbol{v}_h) - \boldsymbol{F}_{\mathrm{RT}_0}(\boldsymbol{v}_h) &\lesssim \|h_{\mathcal{T}}^2 \mathrm{curl}(\boldsymbol{f})\|_{L^2} \|h_{\mathcal{T}}^{-2}(\psi - I_{\mathcal{L}}\psi)\|_{L^2} \\ &\lesssim \|h_{\mathcal{T}}^2 \mathrm{curl}(\boldsymbol{f})\|_{L^2} \|h_{\mathcal{T}}^{-1}\nabla\psi\|_{L^2} \\ &= \|h_{\mathcal{T}}^2 \mathrm{curl}(\boldsymbol{f})\|_{L^2} \|h_{\mathcal{T}}^{-1}\mathrm{curl}\psi\|_{L^2} \\ &= \|h_{\mathcal{T}}^2 \mathrm{curl}(\boldsymbol{f})\|_{L^2} \|h_{\mathcal{T}}^{-1}(\boldsymbol{v}_h - I_{\mathrm{RT}_0}\boldsymbol{v}_h)\|_{L^2} \\ &\lesssim \|h_{\mathcal{T}}^2 \mathrm{curl}(\boldsymbol{f})\|_{L^2} \|\nabla \boldsymbol{v}_h\|_{L^2}.\end{aligned}$$

This concludes the proof. □

Remark 5.3. In the case $k = 2$ this results in a pressure-robust velocity discretisation that converges with the optimal order. The pressure error however may convergence suboptimally, since this relates to testing with non-divergence-free functions. In other words, no improved estimate for the full dual norm $\|\boldsymbol{F}(\boldsymbol{v}_h) - \boldsymbol{F}_{\mathrm{RT}_0}(\boldsymbol{v}_h)\|_{\boldsymbol{V}_h}$ is possible, which is also confirmed by the numerical experiments below.

6. Numerical experiments

This Section studies three numerical examples to confirm that the new approach has optimal convergence rates and is really pressure-robust, opposite to the classical and the enhanced VEM. To conduct the experiments the lowest-order VEM with $k = 2$ is implemented allowing for a RT_1 and RT_0 reconstruction as described in Sections 4 and 5 to keep the optimal order of convergence with respect to the velocity.

Since the discrete solution $\boldsymbol{u}_h$ is still virtual, the errors between the exact solution $\boldsymbol{u}$ and the projection $\Pi_2^\nabla \boldsymbol{u}_h$ are computed, i.e.

$$\|\nabla(\boldsymbol{u} - \Pi_2^\nabla \boldsymbol{u}_h)\|_{L^2}.$$

Moreover, the error will be computed on a series of meshes with different number of degrees of freedom `ndof` to gain convergence rates with respect to $\mathtt{ndof}^{-1/2}$.

In these examples the numerical domain $\Omega = [0,1]^2$ is partitioned into a series of meshes $\mathcal{T}_0, \mathcal{T}_1, \mathcal{T}_2, \ldots$ with the following structure: The unit square is divided into four parts with equal size. The first part consists of (deterministically) distorted quadrilaterals whereas the second part is made of smaller regular squares. Triangles and non-convex pentagons are used to build the third part. Last but not least, the fourth part is constructed using L-shaped polygons including hanging nodes (after the first refinement) and regular squares, see figure 6.1 for the first three meshes.

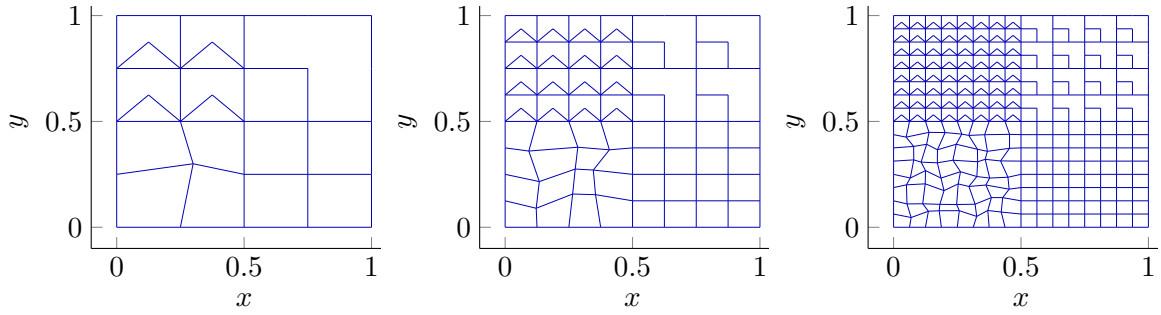

FIGURE 6.1. First three refinement levels $\mathcal{T}_0$, $\mathcal{T}_1$ and $\mathcal{T}_2$ of the meshes used for the computations.

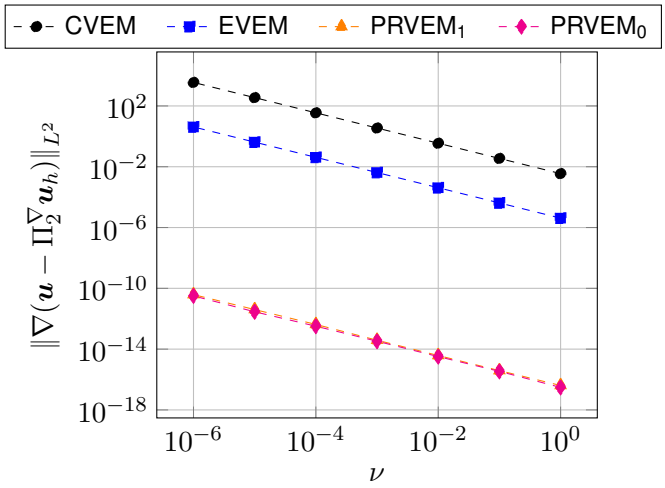

FIGURE 6.2. Dependence of the velocity error on the viscosity computed on the second refinement $\mathcal{T}_2$ of $\mathcal{T}_0$ for different right-hand side discretisations.

6.1. **Hydrostatic problem with different viscosities.** The first experiment is performed only on the third mesh $\mathcal{T}_2$ of Figure 6.1.

The continuous right-hand side is chosen, such that the exact solution reads

$$\boldsymbol{u} = \boldsymbol{0} \in \boldsymbol{V}_h, \quad \text{and} \quad p(x,y) = \sum_{j=0}^{7} x^j y^{7-j} - \frac{761}{1260} \notin Q_h.$$

To show the lack of pressure-robustness of the classical and enhanced VEM the viscosity is varied between $\nu = 10^0, 10^{-1}, \ldots, 10^{-6}$.

All four different right-hand side discretisations are tested: The classical virtual element method (CVEM), the enhanced virtual element method (EVEM), the new pressure-robust version with RT_1 reconstruction (PRVEM$_1$), and the pressure-robust version using the RT_0 reconstruction (PRVEM$_0$).

Figure 6.2 shows the error of the four methods versus the viscosity and visualises the lack of pressure robustness of the classical and the enhanced VEM. The error of the pressure-robust versions are almost zero. The reason that they are not closer to machine precision is that the solver only ensures that the product of the velocity error times ν is close to machine precision.

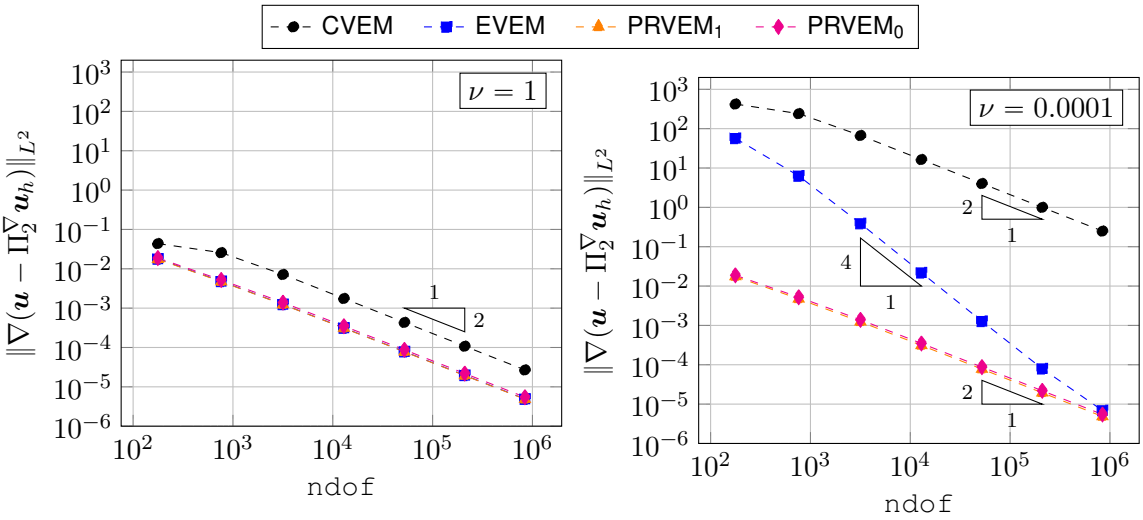

FIGURE 6.3. Convergence history of the velocity error for the second experiment for $\nu = 1$ (left) and $\nu = 10^{-4}$ (right).

TABLE 6.1. Total number of degrees of freedom, pressure error $\|p - p_h\|_{L^2}$ and convergence rates for the experiment of Subsection 6.2 for viscosity $\nu = 1$.

	CVEM		EVEM		PRVEM$_1$		PRVEM$_0$	
ndof	error	rate	error	rate	error	rate	error	rate
177	$1.939 \cdot 10^{-1}$	-	$1.367 \cdot 10^{-1}$	-	$1.367 \cdot 10^{-1}$	-	$2.099 \cdot 10^{-1}$	-
763	$8.535 \cdot 10^{-2}$	1.12	$4.656 \cdot 10^{-2}$	1.47	$4.655 \cdot 10^{-2}$	1.47	$1.072 \cdot 10^{-1}$	0.92
3171	$2.407 \cdot 10^{-2}$	1.78	$1.227 \cdot 10^{-2}$	1.87	$1.227 \cdot 10^{-2}$	1.87	$5.196 \cdot 10^{-2}$	1.02
12931	$6.257 \cdot 10^{-3}$	1.92	$3.126 \cdot 10^{-3}$	1.95	$3.126 \cdot 10^{-3}$	1.95	$2.576 \cdot 10^{-2}$	1.00
52227	$1.579 \cdot 10^{-3}$	1.97	$7.849 \cdot 10^{-4}$	1.98	$7.848 \cdot 10^{-4}$	1.98	$1.289 \cdot 10^{-2}$	0.99
209923	$3.959 \cdot 10^{-4}$	1.99	$1.965 \cdot 10^{-4}$	1.99	$1.964 \cdot 10^{-4}$	1.99	$6.447 \cdot 10^{-3}$	1.00
841731	$9.907 \cdot 10^{-5}$	2.00	$4.913 \cdot 10^{-5}$	2.00	$4.913 \cdot 10^{-5}$	2.00	$3.225 \cdot 10^{-3}$	1.00

6.2. **Vorticity problem with constant viscosity.** The second experiment is conducted on the series of meshes $\mathcal{T}_0, \mathcal{T}_1, \mathcal{T}_2, \ldots$ of Figure 6.1 to obtain convergence rates.

The right-hand side is set in such a way that the exact solution is given by

$$\boldsymbol{u}(x,y) = \begin{pmatrix} -\partial/\partial y \\ \partial/\partial x \end{pmatrix} \left(x^2(x-1)^2y^2(y-1)^2\right) \notin \boldsymbol{V}_h, \quad \text{and} \quad p(x,y) = \sin(2\pi x)\cos(2\pi y) \notin Q_h.$$

For two viscosities $\nu = 1$, $\nu = 0.0001$ the discrete solutions are computed on the first seven levels. The convergence rates for the different viscosities with respect to the total number of degrees of freedom $\mathtt{ndof}^{-1/2} \approx h$ are shown in Figure 6.3.

All methods converge with their expected rates. In particular, the new pressure-robust versions provide significant better results for small viscosities compared to the classical VEM and the enhanced version on coarse grids. As stated earlier the enhanced VEM converges with a convergence rate of 4 as long as the right-hand side discretisation error is dominant, and hence is asymptotically pressure-robust.

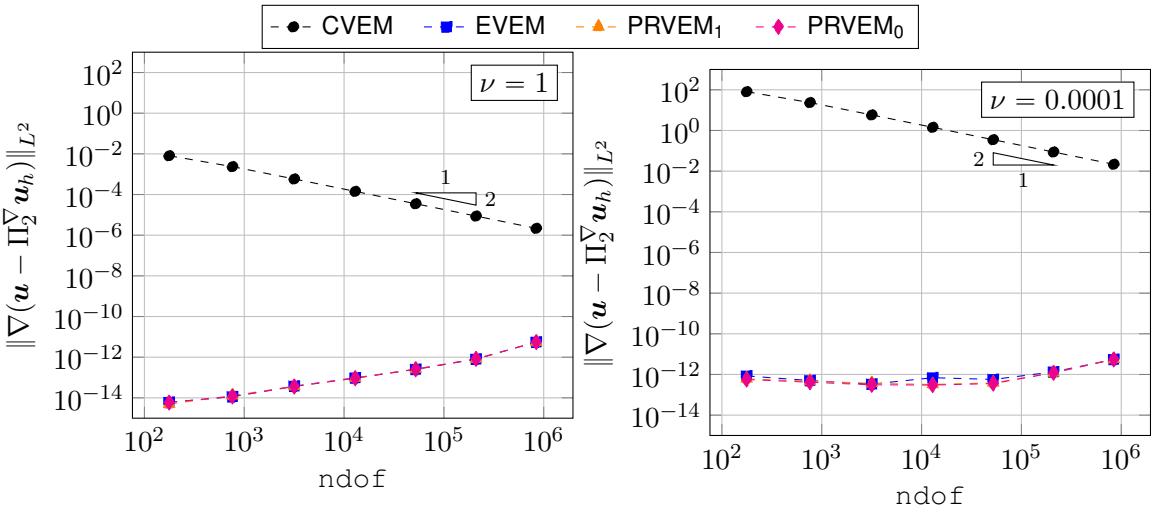

FIGURE 6.4. Convergence history of the velocity error for the third experiment with a linear velocity and quadratic pressure for $\nu = 1$ (left) and $\nu = 10^{-4}$ (right).

As mentioned in Subsection 5.2 the pressure computed by the pressure-robust VEM with RT_0-reconstruction converges only with order 1 in contrast to all the other discretisations which lead to an expected convergence rate of 2. The pressure error and the rate for the different versions computed for $\nu = 1$ can be found in Table 6.1.

6.3. **Potential flows with different polynomial degrees.** As before, the third experiment is performed on the series of meshes $\mathcal{T}_0, \mathcal{T}_1, \mathcal{T}_2, \ldots$ of Figure 6.1.

The exact velocity is prescribed as a polynomial potential flow $\boldsymbol{u} = \nabla r$, i.e. the gradient of a smooth harmonic polynomial $r \in P_s(\Omega)$ of degree s. Then, it holds $\Delta \boldsymbol{u} = \nabla(\Delta r) = 0$ and the pressure is completely determined by the right-hand side. To demonstrate the usefulness of the pressure-robust methods in the Navier–Stokes setting, the right-hand side is chosen to be the convection term

$$\boldsymbol{f} = (\boldsymbol{u} \cdot \nabla)\boldsymbol{u} = \nabla\left(\frac{1}{2}|\boldsymbol{u}|^2\right) = \nabla p$$

which is the gradient of a polynomial $p := \frac{1}{2}|\boldsymbol{u}|^2 + C$ of degree $2(s-1)$, see e.g. [25]. The constant C is fixed by the constraint $\int_\Omega p \, \mathrm{d}x = 0$.

As in the previous experiment, convergence rates of all methods are computed for the viscosities $\nu = 1$ and $\nu = 0.0001$.

6.3.1. *Polynomial degree* $s = 2$. The choice $r = x^2 - y^2$ leads to the linear velocity $\boldsymbol{u}(x, y) := (2x, -2y)^T$ and the corresponding pressure and right-hand side

$$p(x, y) := 2x^2 + 2y^2 - \frac{4}{3}, \quad \text{and} \quad \boldsymbol{f}(x, y) = (\boldsymbol{u} \cdot \nabla)\boldsymbol{u} = (4x, 4y)^T.$$

The convergence rates for all methods for the different viscosities can be found in Figure 6.4. The classical method converges with its theoretically predicted order. In this case, not only the pressure-robust versions but also the enhanced VEM can solve the problem exact up to machine precision, since the right-hand can be exactly approximated.

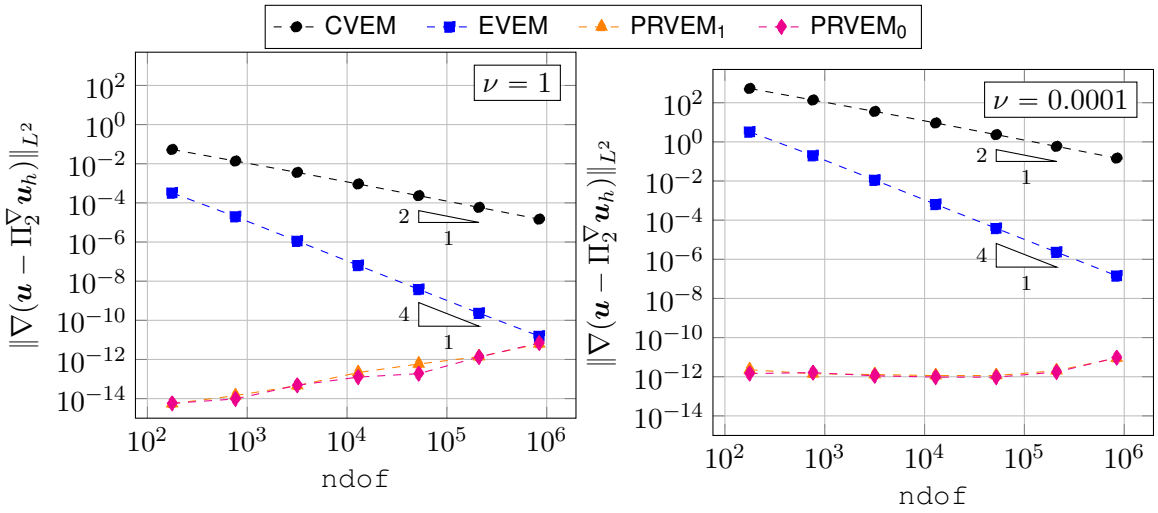

FIGURE 6.5. Convergence history of the velocity error for the third experiment with a quadratic velocity and quartic pressure for $\nu = 1$ (left) and $\nu = 10^{-4}$ (right).

6.3.2. *Polynomial degree* $s = 3$. This time, consider $r = x^3 - 3y^2x$ and the corresponding velocity $\boldsymbol{u} := (3x^2 - 3y^2, -6xy)^T$ with exact pressure and right-hand side

$$p(x,y) := \frac{9}{2}(x^4 + y^4) + 9x^2y^2 - \frac{14}{5}, \quad \text{and} \quad \boldsymbol{f}(x,y) = (\boldsymbol{u}\cdot\nabla)\boldsymbol{u} = 18(x^3 + xy^2, y^3 + x^2y)^T.$$

In Figure 6.5 the convergence rates for all methods for the different viscosities are presented showing optimal convergence rates for the classical and the enhanced VEM as well as the great asset of the pressure-robust version.

On the other hand, this problem indicates also an advantage of pressure-robust methods for the Navier-Stokes setting which is shortly addressed in the outlook.

7. OUTLOOK

This Section discusses several straight-forward extensions of the presented idea.

7.1. **Divergence-free postprocessing.** The quantity $\Pi_k^\nabla \boldsymbol{u}_h$ is in general not divergence-free, but often used as a postprocessing to have some quantity that can be evaluated everywhere. The reconstruction operator $I_{\mathrm{RT}_{k-1}}\boldsymbol{u}_h$ can serve as an alternative divergence-free postprocessing of the discrete solution $\boldsymbol{u}_h$. This might be of importance in coupled multiphysics problems to preserve structural properties like mass conservation [19].

7.2. **Extension to Navier–Stokes.** In the spirit of [19, 25, 2], the reconstruction operator can be also applied in the virtual element discretisation of the Navier–Stokes equations [6]. Then, it appears not only in the right-hand side but also in the material derivative, i.e. time derivative or the nonlinear convection term. A modified computable discrete convection form might read

$$c_h^+(\boldsymbol{w}_h, \boldsymbol{u}_h, \boldsymbol{v}_h) := \int_\Omega (I_{\mathrm{RT}_{k-1}}(\boldsymbol{w}_h)\cdot \boldsymbol{\pi}_{k-1}\nabla\boldsymbol{u}_h) I_{\mathrm{RT}_1}(\boldsymbol{v}_h)\,\mathrm{d}x$$

and a modified discretisation of the time derivative is given by

$$d_h^+(\boldsymbol{u}_h, \boldsymbol{v}_h) := \int_\Omega \frac{\mathrm{d}}{\mathrm{d}t} I_{\mathrm{RT}_{k-1}}(\boldsymbol{u}_h) \cdot I_{\mathrm{RT}_{k-1}}(\boldsymbol{v}_h)\,\mathrm{d}x$$

where $\frac{\mathrm{d}}{\mathrm{d}t}$ can be replaced by any discrete time stepping scheme.

In fact, as demonstrated in [17] for high Reynolds number flows, there are situations where the material derivative $\boldsymbol{u}_t + \boldsymbol{u} \cdot \nabla \boldsymbol{u}$ is (close to) a gradient (in particular for $\boldsymbol{f} = 0$ and $\nu \to 0$) of a possibly non-trivial pressure. Then, a discretisation of the terms in the material derivative based on the divergence-preserving reconstruction operator will be a better choice.

7.3. **Extension to other discretisation schemes on polygonal or polyhedral meshes.** In principle, a similar design of a reconstruction operator is possible for any discretisation on polygonal or polyhedral meshes as long as there is a discretely divergence-free constraint that is satisfied exactly. One example on simplicial meshes can be found in [12] for a discontinuous skeletal method, where also Raviart–Thomas elements are used for a divergence-preserving reconstruction. In [27] a similar divergence-preserving post-processing is used in a projection step of a splitting scheme. Those methods are extendable to general meshes [28] and can then be reconstructed or postprocessed with the subgrid strategy presented here.

References

1. B. Ahmad, A. Alsaedi, F. Brezzi, L.D. Marini, and A. Russo, *Equivalent projectors for virtual element methods*, Computers & Mathematics with Applications **66** (2013), no. 3, 376 – 391.
2. N. Ahmed, A. Linke, and C. Merdon, *On really locking-free mixed finite element methods for the transient incompressible Stokes equations*, SIAM J. Numer. Anal. **56** (2018), no. 1, 185–209. MR 3743746
3. I. Babuska and M. Suri, *On locking and robustness in the finite element method*, SIAM J. Numer. Anal. **29** (1992), no. 5, 1261–1293. MR 1182731
4. L. Beirão da Veiga, F. Brezzi, A. Cangiani, G. Manzini, L. D. Marini, and A. Russo, *Basic principles of virtual element methods*, Mathematical Models and Methods in Applied Sciences **23** (2013), no. 01, 199–214.
5. L. Beirão da Veiga, C. Lovadina, and G. Vacca, *Divergence free virtual elements for the Stokes problem on polygonal meshes*, ESAIM Math. Model. Numer. Anal. **51** (2017), no. 2, 509–535. MR 3626409
6. _____, *Virtual elements for the Navier-Stokes problem on polygonal meshes*, SIAM J. Numer. Anal. **56** (2018), no. 3, 1210–1242. MR 3796371
7. L. Beirão da Veiga, D. Mora, and G. Vacca, *The stokes complex for virtual elements with application to navier–stokes flows*, Journal of Scientific Computing (2019).
8. L. BeirÃčo da Veiga, C. Lovadina, and A. Russo, *Stability analysis for the virtual element method*, Mathematical Models and Methods in Applied Sciences **27** (2017), no. 13, 2557–2594.
9. D. Boffi, F. Brezzi, and M. Fortin, *Mixed finite element methods and applications*, Springer Series in Computational Mathematics, vol. 44, Springer, Heidelberg, 2013. MR 3097958
10. J. Bonelle and A. Ern, *Analysis of compatible discrete operator schemes for the Stokes equations on polyhedral meshes*, IMA J. Numer. Anal. **35** (2015), no. 4, 1672–1697. MR 3407240
11. F. Dassi and G. Vacca, *Bricks for the mixed high-order virtual element method: Projectors and differential operators*, Applied Numerical Mathematics (2019).
12. D. A. Di Pietro, A. Ern, A. Linke, and F. Schieweck, *A discontinuous skeletal method for the viscosity-dependent Stokes problem*, Comput. Methods Appl. Mech. Engrg. **306** (2016), 175–195. MR 3502564
13. D. A. Di Pietro and S. Lemaire, *An extension of the Crouzeix-Raviart space to general meshes with application to quasi-incompressible linear elasticity and Stokes flow*, Math. Comp. **84** (2015), no. 291, 1–31. MR 3266951
14. R. Eymard and R. Herbin, *A staggered finite volume scheme on general meshes for the Navier-Stokes equations in two space dimensions*, Int. J. Finite Vol. **2** (2005), no. 1, 19. MR 2465455
15. R. Eymard, R. Herbin, and J. C. Latché, *Convergence analysis of a colocated finite volume scheme for the incompressible Navier-Stokes equations on general 2D or 3D meshes*, SIAM J. Numer. Anal. **45** (2007), no. 1, 1–36. MR 2285842
16. D. Frerichs, *On pressure-robustness and adaptivity of a virtual element method for solving the Stokes problem*, Master thesis, Humboldt-University of Berlin, September 2019.

17. N. R. Gauger, A. Linke, and P. W. Schroeder, *On high-order pressure-robust space discretisations, their advantages for incompressible high Reynolds number generalised Beltrami flows and beyond*, SMAI Journal of Computational Mathematics **5** (2019), 89–129.
18. V. Girault and P.-A. Raviart, *Finite element methods for Navier-Stokes equations: Theory and algorithms*, volume 5 of Springer Series in Computational Mathematics, Springer-Verlag, Berlin, 1980.
19. V. John, A. Linke, C. Merdon, Michael Neilan, and Leo G. Rebholz, *On the divergence constraint in mixed finite element methods for incompressible flows*, SIAM Rev. **59** (2017), no. 3, 492–544. MR 3683678
20. P. L. Lederer, A. Linke, C. Merdon, and J. Schöberl, *Divergence-free reconstruction operators for pressure-robust Stokes discretizations with continuous pressure finite elements*, SIAM J. Numer. Anal. **55** (2017), no. 3, 1291–1314. MR 3656505
21. P. L. Lederer, C. Merdon, and Joachim Schöberl, *Refined a posteriori error estimation for classical and pressure-robust stokes finite element methods*, Numerische Mathematik **142** (2019), no. 3, 713–748.
22. A. Linke, *On the role of the Helmholtz decomposition in mixed methods for incompressible flows and a new variational crime*, Comput. Methods Appl. Mech. Engrg. **268** (2014), 782–800. MR 3133522
23. A. Linke, G. Matthies, and L. Tobiska, *Robust arbitrary order mixed finite element methods for the incompressible Stokes equations with pressure independent velocity errors*, ESAIM Math. Model. Numer. Anal. **50** (2016), no. 1, 289–309. MR 3460110
24. A. Linke and C. Merdon, *On velocity errors due to irrotational forces in the Navier-Stokes momentum balance*, J. Comput. Phys. **313** (2016), 654–661. MR 3481034
25. ———, *Pressure-robustness and discrete Helmholtz projectors in mixed finite element methods for the incompressible Navier-Stokes equations*, Comput. Methods Appl. Mech. Engrg. **311** (2016), 304–326. MR 3564690
26. A. Linke, C. Merdon, and M. Neilan, *Pressure-robustness in quasi-optimal a priori estimates for the Stokes problem*, arXiv-Preprint (2019), no. 1906.03009.
27. M. Piatkowski and P. Bastian, *A high-order discontinuous galerkin pressure robust splitting scheme for incompressible flows*, arXiv-Preprint (2019), no. 1912.10242.
28. D. A. Di Pietro and A. Ern, *A hybrid high-order locking-free method for linear elasticity on general meshes*, Computer Methods in Applied Mechanics and Engineering **283** (2015), 1 – 21.